Estimating Leaf Area Index from Multiple Return, Small-footprint Aerial LiDAR at the Washington Park Arboretum

Jeffrey J Richardson

A thesis submitted in partial fulfillment of the

Master of Science

University of Washington
2008

Program Authorized to Offer Degree:
College of Forest Resources

University of Washington
Graduate School

This is to certify that I have examined this copy of a master's thesis by

Jeffrey J Richardson

and have found that it is complete and satisfactory in all respects,
and that any and all revisions required by the final
examining committee have been made.

Committee Members:

_____
John A. Wott

_____
Soo-Hyung Kim

_____
L. Monika Moskal

Date:_____

Signature _____

Date _____

TABLE OF CONTENTS

Page

LIST OF FIGURES

Figure Number Page

LIST OF TABLES

ACKNOWLEDGEMENTS

I would like to thank my committee chair and advisor, Dr. John Wott for his choice (and risk) to accept me into the graduate program, his patience when I switched from the professional degree to the academic degree, and his continued support and advice.

I must also offer my deepest thanks to Dr. Soo-Hyung Kim, who advised me on the more technical components of this project, who allowed me to use his laboratory space and equipment, and serve on my committee. Without his contribution, this project would have never begun.

Sincere thanks goes to my third committee member, Dr. L. Monika Moskal, who also provided important technical expertise and encouragement. I have benefited more than most from an extremely helpful and involved committee.

Akira Kato deserves special recognition for his assistance in my field data collection and his mastery of the Total Station. Robert McGaughey helped me in processing the LiDAR data and allowed me to drop in and ask questions when I needed help. Nicole Hackman, Lisa Ciecko, Hannah Kinmonth-Schultz, Emily Palm, Guang Zheng, Todd Erdody, and Joowon Park have all helped me in writing and editing this document.

And lastly I must thank Jeniffer Tobon for field assistance and tolerance of late-evening field work and data processing.

Thank you all.

I. Introduction

This thesis project has explored the utility of using aerial LiDAR (Light Detection and Ranging) to estimate Leaf Area Index (LAI) in a complex urban forest. The project grew out of an initial desire to develop an electronic database of the woody accessions at the Washington Park Arboretum (WPA) in Seattle, WA. It soon became clear that developing this database would be more work than would be appropriate for a thesis, and a more manageable research topic was sought. Initial research led to some of the existing tools used to assess the ecological functions of urban forests, namely iTREE (U.S. Forest Service) and CITYGreen (American Forests) software. Research efforts were concentrated on the iTree software, and in particular the Urban Forest Effects Model (UFORE). Many of the functions of the UFORE model rely on estimates of LAI derived from empirically derived allometric equations (Nowak and Crane, 1998). Specifically, the LAI equations were derived from a single study of open grown deciduous trees (Nowak, 1996), and then applied using correction factors to all other trees. LAI is an important model variable in assessing ecological functions/ecosystem services of urban forests, as it is highly correlated to Gross Primary Productivity (GPP), which in turn is an important variable in determining a forest's capacity to sequester carbon. The amount of rainfall a canopy can intercept and store is also nearly directly proportional to LAI, as total leaf surface area will determine how much water can physically adhere to the leaves' surface. It seemed that a simpler and potentially more precise method of estimating LAI in urban forests could be obtained from LiDAR rather than the allometric method in UFORE, and this was possible because LiDAR datasets had already been acquired in 2004 and 2005 over the WPA. Therefore, this research was undertaken with the goal of estimating LAI from aerial LiDAR.

Aerial LiDAR is a technology that was originally developed to obtain high quality digital elevation models (DEMs), but in the last 10 years LiDAR has also been employed to gain information about the vegetation above the ground. LiDAR works by using a

laser scanner with an integrated receiver. The laser pulses, sending a beam of light into the environment, and that light is scattered, absorbed, or reflected back to the receiver. The receiver detects the light and calculates the distance the light traveled by comparing the amount of time between when the pulse was emitted and when it was received. Most LiDAR lasers, including the one used in this study, utilize a near infrared laser, with a high reflectance for vegetation.

This project began with the objective of creating a novel model to estimate LAI, but after some research, it became clear that there were several different LAI estimation models already proposed in the literature. None had been applied to a heterogeneous urban forest with a large range of LAI values, and it appeared important to assess the accuracy and precision of the different proposed models in such an environment. Since LAI is such an important variable, small changes in LAI can have a large effect on estimates of ecological functions. Therefore, the objective of this thesis project was to (1) compare five methods of estimating LAI, and (2) develop a LAI map that could be used an input into models that can estimate ecological functions.

II. Comparison of Five Methods to Estimate Effective Leaf Area Index from Aerial Discrete-Return LiDAR

1. Introduction

Estimates of forest Leaf Area Index (LAI), defined as the one half the total leaf surface area per unit ground surface area (Asner et al., 2003), are important input parameters for a wide range of ecological models (Gower et al., 1999; Hanssen and Solberg, 2007; Melillo et al., 1993), but arriving at estimates over large spatial scales has proven difficult due to limitations in time, cost, and accuracy. LAI is commonly estimated using Beer's Law by hemispherical photographs or the LAI-2000 (LiCOR, inc.)(Gower et al., 1999), but these two methods are only useful for small areas due the time required in acquiring and processing the data. Indirect techniques utilizing remote sensing to estimate LAI show the most promise for delivering accurate estimates at larger spatial scales. Existing techniques fall into two main categories: (1) passive optical remote sensing, which tends to be limited in the range of LAI values it can accurately estimate do to saturation effects when relying on indices such as the Normalized Vegetation Difference Index (NDVI) (Gower et al., 1999; Lüdeke et al., 1991) and (2) active LiDAR remote sensing, which has been shown to be successful on a limited range of LAI values and/or for homogenous, single species dominated stands (Lim et al., 2003; Morsdorf et al., 2006; Riaño et al., 2004; Solberg et al., 2006). Most studies have derived the effective LAI (LAI_E), which does not correct for the non-random distribution of foliage or the presence of non-foliage elements (eg: branches, bark) in the canopy. Indirect methods based on Beer's Law also calculate LAI_E. In order to arrive at true LAI, one would need to perform corrections, these methods have been well studied (Chen et al., 1997; Leblanc et al., 2005), and are outside the scope of this study.

Aerial LiDAR utilizes an airplane or helicopter mounted scanning laser with an integrated GPS unit to collect three-dimensional data points (Lefsky et al., 2002). The

characteristics of the final dataset depend on various parameters such as the height of the aircraft, diameter of the LiDAR laser beam, scanning nadir angle, and processing equipment. Large footprint, full-waveform LiDAR utilizing the SLICER instrument has been shown to be capable of estimating LAI in Douglas-fir/Western-hemlock dominated forests (Lefsky et al., 1999), but the instrument is not widely available and is unable to give information at high spatial resolution. Small-footprint, multiple return systems are more widely available, and have been shown to be capable of estimating LAI_E in single-species dominated stands and/or in stands with a small range of LAI_E values (Lim et al., 2003; Morsdorf et al., 2006; Riaño et al., 2004; Solberg et al., 2006). Table 1 summarizes the range of ground based LAI_E values used in these studies, the dominant tree species, and the model found to best fit their ground-based LAI_E estimates. Each study used a different method to estimate LAI_E, suggesting that various methods may provide accurate estimate of LAI_E in homogenous forests with small LAI_E values and ranges. It is not known, however, which models can best predict LAI_E in a more heterogeneous, mixed forest with a wide range of LAI_E values.

Table 1: Summary of different methods to estimate LAI from aerial LiDAR

Study	Range of LAI values	Forest Type(s)	Best LAI_E model[a]
Lefsky et al., (1999)	0-14	Douglas-fir/Western hemlock	$LAI = \alpha + \beta(FCV - CGV - CC/H)$
Lim et al., (2003)	0.5-4	sugar maple/yellow birch	$LAI_E = \alpha + \beta MRE$
Riaño et al., (2004)	0-≈3	Pyrenean oak and Scots pine	$LAI_E = \alpha + \beta PCH$
Morsdorf et al., (2006)	0-2	mountain pine/stone pine	$LAI_E = \alpha + \beta F_c (\sum R_{CF}/(\sum R_{CL} + \sum R_{CO}))$
Solberg et al., (2006)	0-1.6	Scots pine	$LAI_E = \beta - \ln(R_G/R_C + R_G)$

[a]Model variables are described in Appendix A

The aim of the present study was to (1) obtain LAI_E estimates in a highly variable forest composed of multiple coniferous and deciduous species with a wide range of LAI_E

values, (2) determine the best method for comparing LiDAR derived metrics and indirect field measurements, (3) evaluate the five different models proposed for estimating LAI_E using aerial LiDAR, and (4) identify the best model and determine the effect of spatial extent on the model predictions.

2. Materials and methods

2.1. Study site

The present work was conducted at the Washington Park Arboretum (WPA) in Seattle, WA (Fig. 1). The WPA is a 230 acre (0.931 km^2) forest managed by the University of Washington Botanic Gardens. The forest is comprised of over 4000 individual species of tree or shrub, but dominated by a native matrix of Douglas-fir (*Pseudotsuga menziesii),* Western hemlock (*Tsuga heterophylla),* Western red-cedar (*Thuja plicata),* and big leaf maple (*Acer macrophyllum)*. An 86 acre (0.347 km^2) subsection of the WPA was used for the present work (Fig. 1.c,d.), consisting of areas with slopes less than 10%, not located on trails, at least 10 m from park boundaries, and away from buildings. Within this subsection, 100 plot locations were randomly located within five stratified fractional cover classes during the summer of 2007. Hemispherical photographs were not collected on two points due to the onset of autumnal leaf senescence, reducing the total number of points to 98 (Fig. 1.c). At each point, 250 individual GPS points were averaged using a Trimble GeoXT (Trimble Navigation Ltd.) operating in DGPS mode.

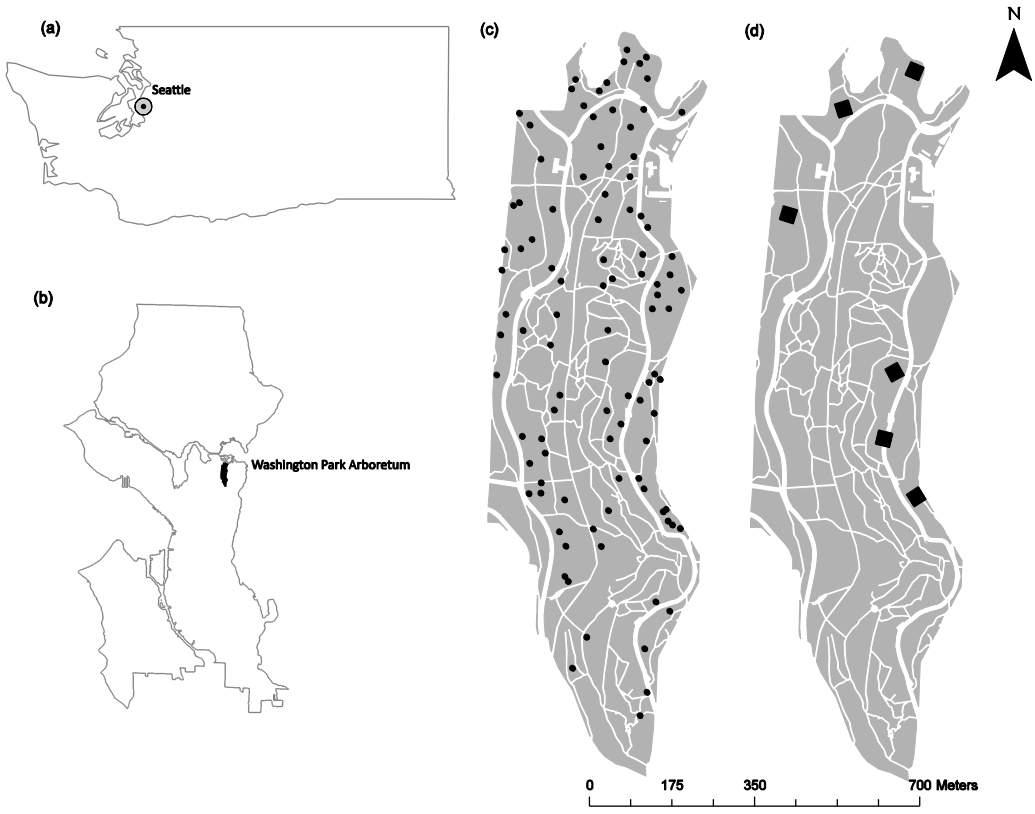

Figure 1 : (a) The state of Washington, with the city of Seattle shown by the dotted circle, (b) The city of Seattle with the WPA in black, (c) the WPA and the 98 points, and (d) the WPA and the six 30 by 30 m plots

Six separate 30 by 30 m plots were installed in the WPA in the summer of 2007, with two plots composed of all conifers, two all deciduous, and two mixed conifer and deciduous (Fig. 1.d). A Nikon DTM 420 Total Station (Nikon, corp.) and Trimble XR Pro GPS (Trimble Navigation Ltd.) were used to capture the geographic coordinates of the four plot corners and check for square. A 5 by 5 m grid was set up over each plot for the purpose of obtaining indirect LAI_E estimates that could be aggregated for plot wide estimates.

2.2. Ground estimates of LAI_E using hemispherical photography

Hemispherical photographs were captured at each of the 98 points and at each grid intersection (a total of 49 photographs) in the six 30 by 30 m plots between June and August of 2007. All photographs were taken before sunrise, after sunset, or under uniformly overcast skies using a Nikon CoolPix 4500 (Nikon, corp.) leveled on a tripod one meter above the ground. At each point, a single hemispherical photograph was obtained utilizing the methodology of Zhang et al. (2005) to find the optimum exposure time. Photographs were processed using the Digital Hemispherical Photography (DHP) software (Leblanc, 2006), which breaks the photograph into ten annulus rings, with each ring corresponding to 9° of zenith angle, beginning with 0-9° at ring one. Rings 9 and 10 were excluded from all analysis due to the influence of topography on the LAI_E estimates. Hills would have been counted as foliage if these rings were not excluded. Eight different LAI_E estimates were obtained using DHP for each photograph, corresponding to the inclusion of ring one, ring one and two, and so on until the eighth estimate included rings one through eight. These estimates were obtained in order to find the best relationship between the conical view of the hemispherical photograph and LiDAR metrics obtained from a cylinder, as has been performed previously (Morsdorf et al., 2006). As noted in the introduction, the photographs estimate effective LAI, and in this study, LAI_E was not corrected in order to estimate the true LAI, as the LiDAR based estimates would likely require the same correction factors. The LAI_E estimates, therefore, must be carefully examined and possibly corrected before they are used in an ecological model.

2.3. Ground estimates of LAI_E using the LAI-2000

Estimates using the LAI-2000 (LiCOR, inc.) were obtained at each of the 98 points under the same sky constraints as the hemispherical photographs between June and August of 2007. Time constraints did not allow for measurements at the 30 by 30 m plots. With only one instrument, it was necessary to modify the collection technique in

accordance with the instrument manual by installing a 45° viewcap and bringing the instrument into an open area to obtain "above canopy" readings. The viewcap allowed the reading to be taken in areas with smaller canopy gaps, as the sensor rings only needed to be exposed to open sky conditions in a much smaller field of view. After an "above canopy" reading was obtained, the instrument was quickly brought to the point location where eight readings were taken in 45° increments. A final "above canopy" reading was then taken in order to reduce error caused by changing sky conditions. The LAI-2000, like the hemispherical photographs, produces estimates of effective LAI, and no additional analysis was performed on the LAI_E estimates obtained aside from the calculations performed by the instrument's internal hardware.

2.4. Interpolation of LAI_E at 30 by 30 m plots

In order to arrive at plot level estimates that could be easily subdivided into smaller spatial areas, the 49 individual hemispherical photograph LAI_E estimates for each 30 by 30 m plot were interpolated to a raster using the Inverse Distance Weighted (IDW) function available in ArcGIS 9.2 (ESRI, corp.). The interpolation allowed the 30 by 30 m plots to be subdivided into smaller areas where individual mean LAI_E estimates could be calculated. IDW interpolation produced a surface that more accurately reflected the natural LAI_E variation in the plots than Kriging or the Spline function.

2.5. LiDAR data acquisition and processing

Aerial discrete-return LiDAR coverage was obtained over the WPA on August, 31st, 2004 using an Optech ALTM 30/70 laser scanner at an elevation of 1200 m above ground with a maximum scan angle of ± 10° from nadir. The scanner classified the LiDAR returns into 1st, 2nd, 3rd, and Last, where Last was the final return to break the instrument's energy threshold, regardless of return number. The last return may have been a fourth return, but no data was collected for only fourth returns. Therefore, last returns were excluded from the analysis. The raw LiDAR data was processed using Fusion software's ClipData feature (McGaughey, 2007) to normalize the vegetation

heights above a constant ground elevation using a ground model previously developed from the LiDAR data. This produced a dataset where the Z value for each point represents the true elevation of that point above ground level.

2.6. Computation of LiDAR metrics

For each of the 98 plots, cylindrical LiDAR point clouds of 2.5, 5, 10, 15, 20, and 25 m radius were extracted. Within each of these cylinders, various metrics were calculated: the number of returns above 2 m in elevation (R_C), the number of returns below 2 m (R_G), the mean elevation of all returns (MRE), total canopy 1st returns (C_{R1}), canopy 2nd returns (C_{R2}), and canopy 3rd returns (C_{R3}). Fractional canopy cover (F_c) was estimated by rasterizing the LiDAR dataset according to the maximum elevation of each grid cell. All grid cells with values greater than 2 m were considered canopy, while those less than 2 m were considered ground. The proportion of canopy grid cells within each 10 m radius circle was calculated for each of the 98 points, and used as the estimate of F_c. The metrics of closed gap volume (CGV) and canopy classes (CC) could not be derived, as full waveform LiDAR was not available. Therefore, to approximate the Lefsky et al. (1999) model, a canopy volume metric (CV) was derived by creating a Triangular Irregular Network (TIN) surface from the maximum height of the LiDAR points using ArcGIS 9.2 (ESRI, corp.). CV was estimated using the surface volume tool in ArcGIS 9.2. The tool calculates the volume between the TIN canopy surface and the ground surface determined by the ground model.

2.7. Statistical analyses

All analyses were performed using R version 2.6.2. Simple linear correlation analysis was performed between the 98 hemispherical photograph LAI_E estimates and 98 LAI-2000 estimates. Hemispherical photograph estimates, which were the better predictors of LAI_E (see results), were then used in subsequent analyses. Simple linear regression was carried out to determine which LAI_E estimate using the model of Solberg et al. (2006) computed from differing LiDAR cylinder radii was best correlated to LAI_E

estimates derived from different combinations of hemispherical photograph annulus rings, as has been previously similarly performed (Morsdorf et al., 2006; Riaño et al., 2004). This radius and annulus ring combination was then used in all subsequent analyses. Each computed LiDAR metric was then input into the five models described in Table 2 and analyzed using simple linear regression of the hemispherical photograph LAI_E estimates taken at each of the 98 points.

To evaluate the relationship between spatial extent (and thus number of LiDAR points used to compute the metrics) and predictive accuracy, the 30 by 30 m plots were broken into smaller areas: 15 by 30 m, 15 by 15 m, and 7.5 by 7.5 m. LAI_E was then predicted for each of these areas using the best model chosen by the process above, and compared to the average LAI_E determined from the mean interpolated raster values for the same area.

3. Results

3.1. Determination of best indirect method

Comparisons between hemispherical photography and the LAI-2000 showed good correlation (Figure 2, R^2 0.804), although the LAI-2000 produced larger estimates at low LAI_E values, while hemispherical photographs produced larger estimates at high LAI_E values. It was necessary to determine which of the two methods of LAI_E estimation would be best correlated to the LiDAR metrics. Both the LAI-2000 and hemispherical photograph LAI_E estimates (results not shown) were compared to each of the different models for estimating LAI_E from LiDAR. In all cases, hemispherical photographs were slightly more correlated, and thus were used for all subsequent analyses.

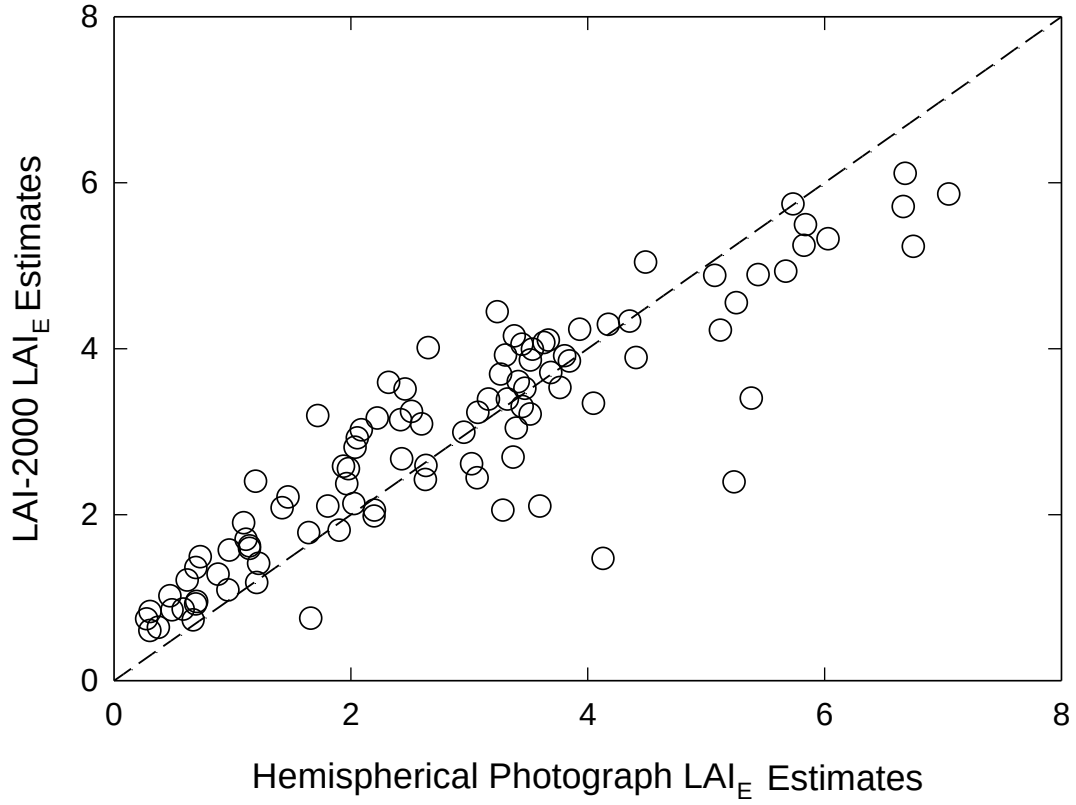

Figure 2: Comparison of hemipsherical photograph LAI_E estimates and LAI-2000 estimates at the 98 plots within the Washington Park Arboretum. One to one relationship shown by the dotted line.

3.2. Determination of best LiDAR cylinder radius and hemispherical photograph annulus ring combination

Initially, simple linear regression was used to compare the different LiDAR LAI_E models using LiDAR metrics extracted from a cylinder with 15 m radius, chosen based on previous studies (Morsdorf et al., 2006; Riaño et al., 2004), to hemispherical photograph LAI_E estimates using all eight annulus rings. Model E proved to be most highly correlated, and this model was used to obtain coefficients of determination from the simple linear regressions of the six different LiDAR cylinder radii (2.5, 5, 10, 15, 20, 25 m) and eight different hemispherical photograph annulus ring combinations (1, 1-2, 1-3, 1-4, 1-5, 1-6, 1-7, 1-8)(Fig 3.). Intercept estimates were included in the regressions in

order to arrive at comparable estimates of the coefficient of determination. Because Model E is logarithmic, several datapoints at 2.5 and 5m cylinder radii were excluded because they contained no ground returns. Therefore, coefficients of determination at these radii are likely overestimated, although this did not influence our final combination. The series of simple regressions found the 10 meter segment radius and the annulus ring 1-7 combination to be the best correlated (R^2 0.6782), and this combination was used for all subsequent analyses.

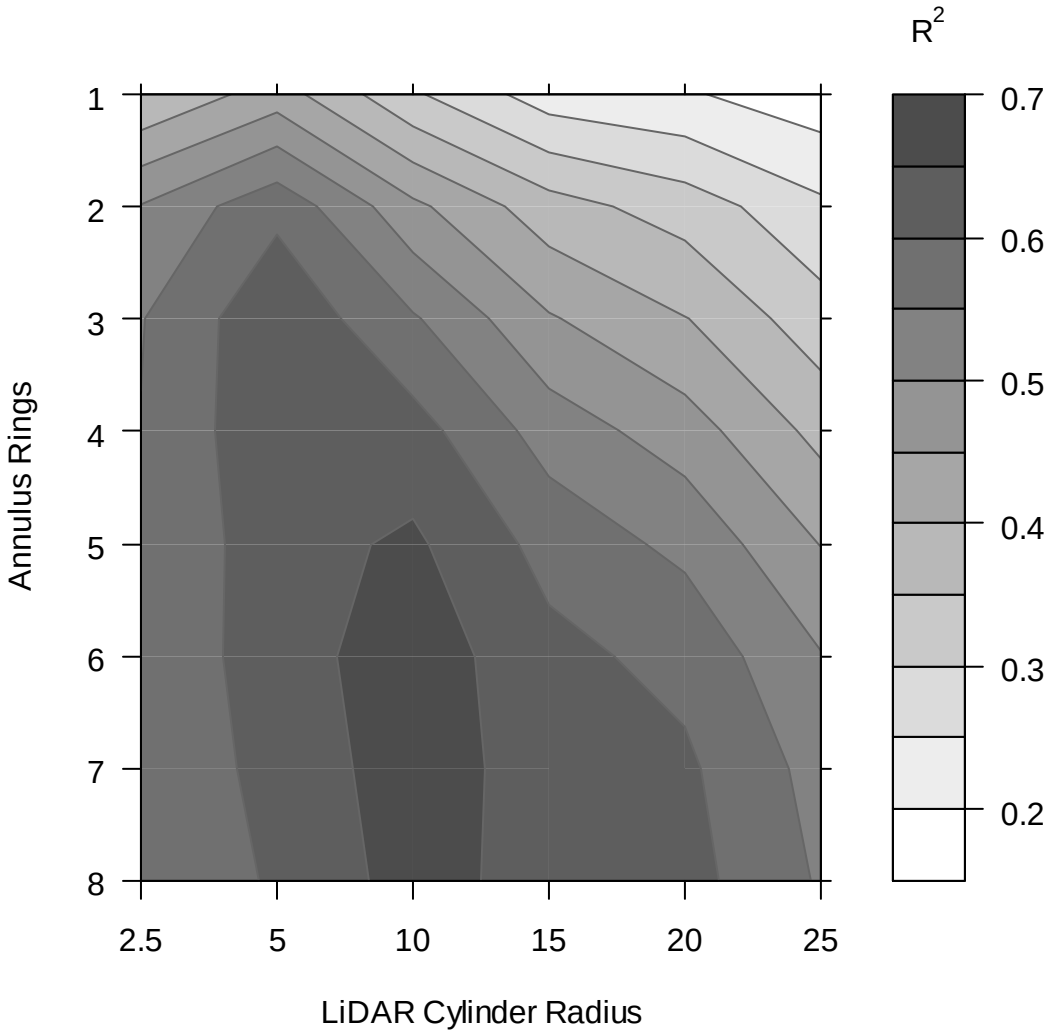

Figure 3: Contour plot of the of the coefficient of determination resulting from simple linear regressions of model E with an intercept value included at differing annulus rings and LiDAR cylinder radii at 98 points in the Washington Park Arboretum.

3.3. Comparisons of LiDAR estimation models

Table 2 summarizes the results of the simple linear regressions of the five models investigated. Each model is given an identifier, and will be thus referred to by that identifier. Thirteen observations were excluded from the regression of the Model D, as they were apparently outside the sensitivity of the model as the inclusion of those observations reduced the coefficient of determination to 0. The coefficients from Table 2 were used to produce predictions of LAI_E using the 5 models (Fig.4). Model E was most highly correlated to hemispherical photograph estimates of LAI_E, and produced the least amount of residual scatter at high LAI_E.

Table 2: Results of simple linear regression between LAI_E estimation models and hemispherical photograph LAI_E estimates

Identifier	**Reference/ Metric**	**Model**[a]	**Number of Observations**	**α (SE)**	**β (SE)**	**R^2**
A	Lim et al. (2003)	$LAI_E = \alpha + \beta MRE$	98	0.52156 (0.28504)	0.20985 (0.2267)	0.4717
B	Canopy Volume	$LAI_E = \alpha + \beta CV$	98	0.72655 (0.24877)	6.5269×10^{-3} (6.552×10^{-4})	0.5083
C	Riaño et al., (2004)	$LAI_E = \alpha + \beta 100(F_C / F_c + F_g)$	98	-1.42509 (0.38287)	0.05850 (0.00497)	0.5907
D	Morsdorf et al., (2006)	$LAI_E = \alpha + \beta F_c (\sum R_{C1}/(\sum R_{C2} + \sum R_{C3})$	85	0.9472 (0.5899)	0.9675 (0.2624)	0.1408
E	Solberg et al., (2006)	$LAI_E = \beta - \ln(R_G/R_G + R_C)$	98	-	1.6852 (0.05161)	0.6756

[a]Model variables are described in Appendix A

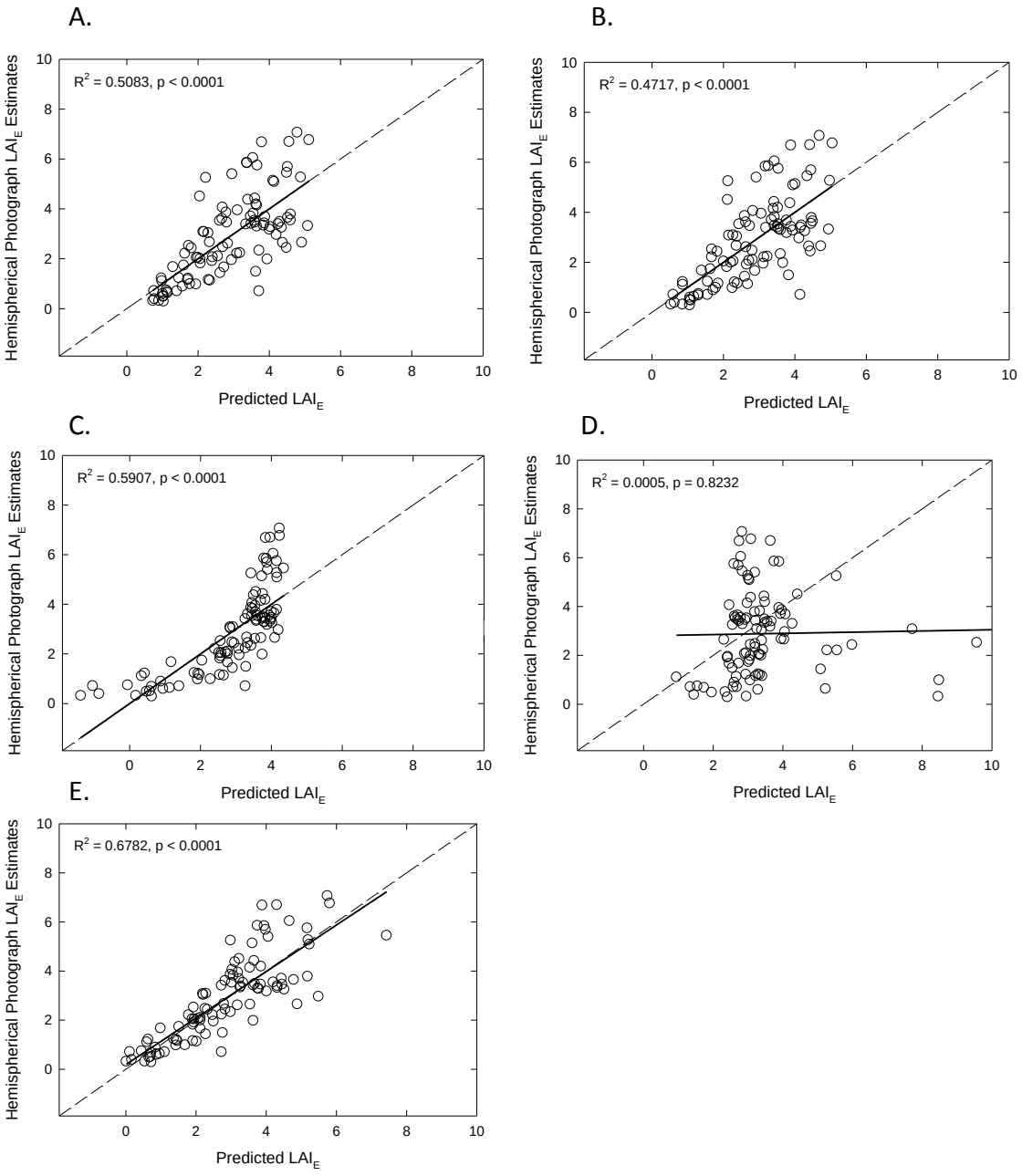

Figure 4: Simple linear regression of predicted values of Models A-E with parameters from Table 2 against hemispherical photograph estimates of LAI_E . Note that one data point is not shown in 4.D. In each graph, the dotted line represents the 1:1 relationship, and the dark line is the best fit.

3.4. The relationship between spatial extent and model accuracy

Model E with the parameters from Table 2 was used to predict LAI_E at the six 30 by 30 m plots. Individual estimates were obtained at each 30 by 30 m area per plot, two 30 by 15 m areas per plot, four 15 by 15 m areas per plot, and sixteen 7.5 by 7.5 m areas per plot. Fig. 5 shows the comparison of those predictions to the interpolated LAI_E estimates for each area. At the smallest spatial extents, several of the subplots contained no ground LiDAR returns, and were excluded from the analysis. The coefficient of determination was also calculated for each of the four spatial extents by performing simple linear regressions of the model predictions and the interpolated LAI_E estimates. Because of the omission of several subplots at the smallest spatial extent due to presence of no ground returns, the coefficient of determination is likely an overestimate for the 7.5 by 7.5 m areas. The inset in Fig. 5 shows that predictive accuracy increases linearly with increasing spatial extent.

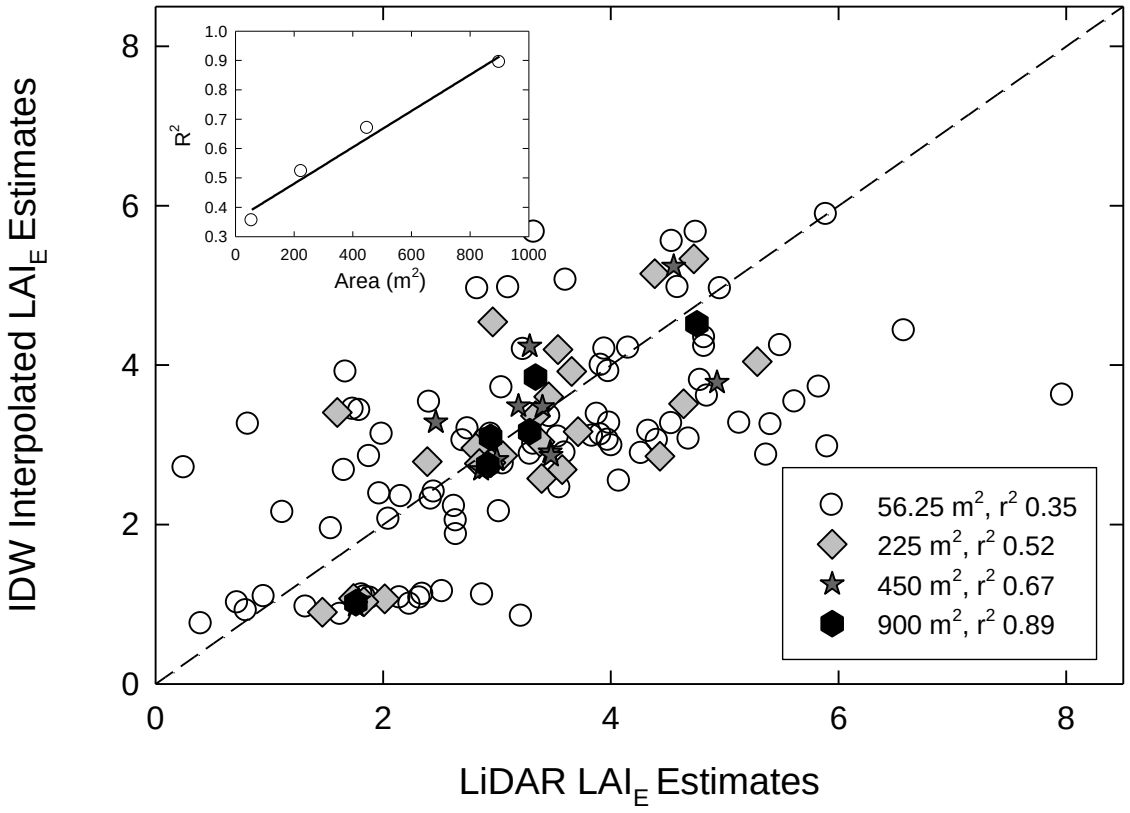

Figure 5: Prediction of Model E at six 30 by 30 m plots in the WPA. Predictions are made at four spatial extents, and the relationship between spatial extent and the correlation coefficient is shown in the inset graph.

4. Discussion

4.1. Comparison between hemispherical photographs and the LAI-2000

The good correlation between the hemispherical photograph and LAI-2000 estimated LAI_E is not surprising, as they both estimate LAI_E based on Beer's Law (Monsi and Saeki, 1952). The slightly higher LAI_E estimates of the LAI-2000 at low LAI_E levels is likely a cause of the ability of that instrument to better discern above and below canopy light intensity differences. Vegetation bordering bright open sky will tend to be underestimated using hemispherical photographs due to the penumbra effect. The

cause of the opposite difference at higher LAI_E levels between the two methods is less clear. At high LAI_E levels, small differences in open sky patches can have a large effect on LAI_E estimation, but it is unclear if or why there is a systematic difference between the two methods.

4.2. The relationship between LiDAR cylinder radius and the combination of hemispherical photograph annulus rings

The best correlated combination of LiDAR radius and hemispherical photograph annulus ring combination closely matches what has been previously found (Morsdorf et al., 2006; Riaño et al., 2004). Attempting to correlate LAI_E estimates based on gap fraction estimates from radiation captured from a conical area of the sky to a cylindrical LiDAR point cloud will always result in some error. In a heterogeneous forest such as the WPA, this error is magnified as there is a high probability that areas at the far edge of the photograph's conical view will different than the areas in the middle which more closely relate to the cylindrical LiDAR point cloud. This error contributes to the residual errors seen in Fig. 4.

The cost effectiveness and relative speed at which hemispherical photographs can be acquired will continue to make them an attractive method for obtaining ground based estimates of LAI_E, but the inherent error of matching a cone to a cylinder suggests that the upper bound of potential correlation between photographs and LiDAR may have already been reached. Future studies should concentrate on methods to arrive at the true LAI within the cylindrical space around a point. One potential next step would be to simulate canopy structure in a computer environment and simulate LiDAR behavior within that environment.

4.3. The distinction between the two main LAI_E estimation methods

As noted in the introduction, ground-based indirect LAI estimation falls into two main categories: allometric methods and methods based on Beer's Law. Allometric methods tend to be applicable for a single species in a single geographical area, and

when allometric equations are applied to trees outside of that narrow range, their accuracy decreases (Gower et al., 1999). In Fig. 4, the two models based on biophysical variables, model A and B, experience rapidly increasing residual error at LAI_E values greater than 2. This is not surprising as this is essentially an allometric approach to estimating LAI_E. If the WPA was dominated by a single species, these models would be expected to predict very accurate values of LAI_E, but since it is very heterogeneous, the relationship between volume and height and LAI_E differs greatly amongst species, accounting for the large residual errors. While this suggests that these models may be appropriate to predict LAI_E in homogenous forests, they still need calibration by ground-based LAI estimation methods in order to estimate regression coefficients, which adds time and cost to the use of this method for larger spatial scales.

The Beer's Law based methods, conversely, produce LAI_E estimates by arriving at the difference between above and below canopy light levels, shown by the following equation:

$$I = I_0 e^{-KF} \quad (1)$$

where *I* is the below canopy light intensity, I_0 is the above canopy light intensity, *F* is the LAI_E, and *K* is the extinction coefficient (Monsi and Saeki, 1952). As Solberg et al. (2006) noted, this equation can be rewritten in the form:

$$F = -\frac{1}{K} \ln I/I_0 \quad (2)$$

and the proportion of LiDAR ground returns to total LiDAR pulses emitted can be substituted for I/I_0:

$$F = -\frac{1}{K} ln(Ground\ Returns/Canopy\ Returns\ + Ground\ Returns) \quad (3)$$

This method has several benefits compared to the allometric models. It is much less sensitive to species differences, resulting in less residual error as can be seen in Fig. 4.E. It also does not necessarily require model calibration, as there is a body of literature describing the extinction coefficient of various forest types (Monsi and Saeki, 1952; Pierce and Running, 1988; Thomas and Winner, 2000). Using the inverse of the

regression coefficient from model E. (2006) from Table 2, the estimated extinction coefficient is 0.5934. While this value will likely differ in different forest types, it tends to fall within the range of 0.5-0.7 (Pierce and Running, 1988; Vose et al., 1995), and utilizing a value of 0.6 is reasonable in a heterogeneous forest such as the WPA. One of the limitations of utilizing Beer's Law is that it produces estimates of LAI_E and must be corrected. Applying multiple correction factors for the many different species in a heterogeneous forest is not realistic if one is attempting to estimate LAI for very large spatial scales, and further research is necessary to examine whether clumping indices and the ratio of bark to foliage can be directly estimated from aerial LiDAR.

LiDAR intensity values present a potential source of data from which to differentiate foliage returns from bark/wood returns. Different objects reflect differing wavelengths of light differently, and this is the basis of most optical remote sensing. The wavelength of the laser used would have a large effect on any model developed using this technique, and perhaps the best solution would be to develop a LiDAR system that uses multiple wavelengths of lasers.

4.4. The saturation problem and potential solutions

Although the Beer's law method represented by equation 3 was the best method for estimating LAI_E from aerial LiDAR in the WPA, residual error still increased with increasing LAI_E. There are two likely causes for this behavior. First, the error associated with comparing the conical view of the hemispherical photograph to the cylindrical LiDAR point cloud will likely increase with increasing LAI_E. At high LAI_E, small differences in gap fraction can lead to large changes in LAI_E derived from hemispherical photographs. As noted in section 4.5, there were many point locations where dense forest patches were bordered by open areas due to the heterogeneous nature of the WPA. In these areas, the LiDAR cylinders captured only dense vegetation, while open sky at the edges of the photographs increased the gap fraction, leading to error. The opposite occurred in open areas ringed by dense vegetation. Secondly, because the

model is comparing canopy to ground returns, the model loses sensitivity in areas where there are no ground returns. Using a 10 m cylinder radius, there were no points that contained only canopy returns, but there were smaller areas within those cylinders that contained very dense vegetation with no ground returns. This is an issue that is also found in satellite based remote sensing using the Normalized Difference Vegetation Index (NDVI)(Wang et al., 2005):

$$NDVI = \frac{R_{NIR} - R_{VIS}}{R_{NIR} + R_{VIS}} \quad (4)$$

Where R_{NIR} and R_{Vis} are the reflectances derived from a satellite's near-infrared and visible bands respectively. NDVI is driven by the difference in reflectance between vegetation and ground, and when vegetation reaches a certain density, around a LAI of 3 (Lüdeke et al., 1991), this index no longer changes because the soil is mostly covered by vegetation. The same problem is observed with LiDAR. As the gap fraction decreases, the probability of an individual laser pulse penetrating through a gap and reflecting off the ground with enough energy to be recorded by the laser scanner decreases exponentially. Hence, the residual error in Fig. 4.B. begins to increase around LAI_E of three.

There are four main ways this saturation problem can be overcome. (1) One can increase the number of laser pulses per square meter. This will increase the likelihood that a pulse will find a gap. (2) One can increase the spatial extent from which one is computing the number of ground and canopy returns. Fig. 5 illustrates this effect, as at larger areas there is a greater probability that an individual laser pulse will strike a canopy gap, yielding more ground returns. (3) The off-nadir angle of each individual laser pulse could be included as a variable in a model. At larger off-nadir angles, the laser beam may pass through gaps that would not be visible at very small off-nadir angles. It would be important to correct for the reduced probability of striking the ground at large off-nadir angles, though, as the path length would be increased, thus increasing the probability that light would be attenuated. (4) One could reconfigure the

LiDAR instrument to be more sensitive to low energy reflections or reduce the beam diameter. It is highly likely that laser pulses are penetrating through very small gaps, but that there is not enough reflected energy to be recorded by the scanner. As LiDAR technology matures, forestry specific instruments and calibrations should be developed to increase the sensitivity to low energy ground returns. At present, though, most advances in LiDAR technology center around increasing the scanning frequency.

Even with improvements to correct the saturation problem, estimating LAI_E using Beer's Law will never give the absolute true LAI. Extremely dense areas of foliage that overlap will absorb all light, ensuring that no LiDAR pulses will reach the ground. In these areas, scanners that can partially penetrate foliage may provide the ultimate solution to achieving true LAI. Both long and short-wave radiation is transmitted through foliage, and sensors operating in these wavelengths may provide areas for future research.

4.5. Conclusions

The various models that have been developed to estimate LAI_E from aerial LiDAR fall into two categories: allometric and Beer's Law based methods. Each main method has its limitations, with allometric models only applicable to single species dominated stands and dependent on calibration utilizing ground-based methods, while Beer's Law based methods exhibit saturation at high LAI_E values and do not correct for foliage clumping or presence of non-foliage elements. In a heterogeneous forest, the Beer's Law method clearly produces more accurate predictions of $LAI_{E,}$ and also does not require calibration as the extinction coefficient, k, can be approximated by using a value of 0.6. Continued research should be performed to examine the influence of different scanner types on LAI_E estimation, as well as research into the possibility of deriving the clumping index and bark to foliage ratio from LiDAR data.

III. Estimation of Effective Leaf Area Index at the Washington Park Arboretum

After selecting the best model for estimating LAI_E at the WPA, it was possible to produce estimates of LAI_E for the entire WPA. Interpretation of the estimates should be limited to the subset of the WPA that was included in the development of the model, as the model was parameterized using this specific area (Fig. 1). It may be reasonable to expect the model will still perform reasonably well outside of the study area, but only estimates within the bounds of the study area should be used without further investigation and validation.

The final area-wide estimates of LAI_E were produced in map form using ArcGIS 9.2. (ESRI, inc). By creating two separate raster grids where each pixel was equal to the sum of ground or canopy returns within the extent of that pixel, it was possible to create a separate raster grid equal to the output of Model E with the parameters from Table 2. The pixel size was set at 5m in order to obtain a reasonably high resolution map that could display the heterogeneity of LAI_E values at the WPA. This raster grid could then be displayed in ArcGIS 9.2 (Fig 6.), but contained several areas of no data (shown as white areas in the map) due to the fact that many raster pixels contained no ground points, because of the saturation effected discussed above.

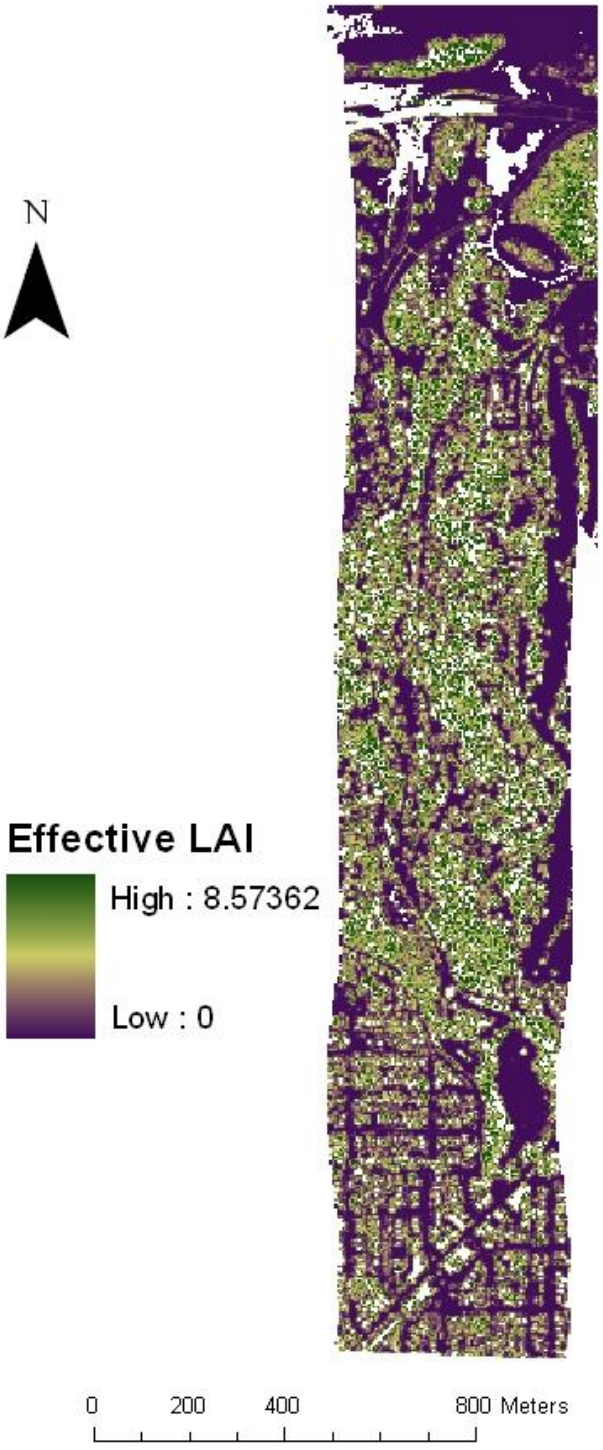

Figure 6: Estimates of LAI_E for the entire extent of the 2004 LiDAR acquisition. White areas indicate areas where there were no ground returns within the pixel.

Several methods have been employed to create an LAI_E map for the study area at the WPA, within the context of attempting to minimize errors brought on by the saturation effect, while attempting to maximize the resolution. First, the grid from Fig. 6 was simply clipped to the extent of the study area, keeping the same pixel size of 5 m (Fig 7.a.). This may be the most objective presentation of the model output, but it would impossible to use this grid as a source of LAI_E for another model because of the many areas of missing data. The missing data pixels should contain the largest values of LAI_E, and to leave those pixels out a model to estimate rainfall interception, for example, would result in large underestimates.

Figure 7.b. is a map displaying interpolated LAI_E created by setting no data pixels set to a value of 9. Although 9 is somewhat arbitrary, it was chosen because it was assumed that the pixels of no data contained larger LAI_E values than the maximum of 8.16 found within the study area. A value of 9 was larger, but still physically feasible. IDW interpolation was run on the grid from Figure 7.a. with the no data values set to 9 to produce Figure 7.b. While there is some error associated the arbitrary assignment of 9, this grid can act as a source of continuous data for ecological models.

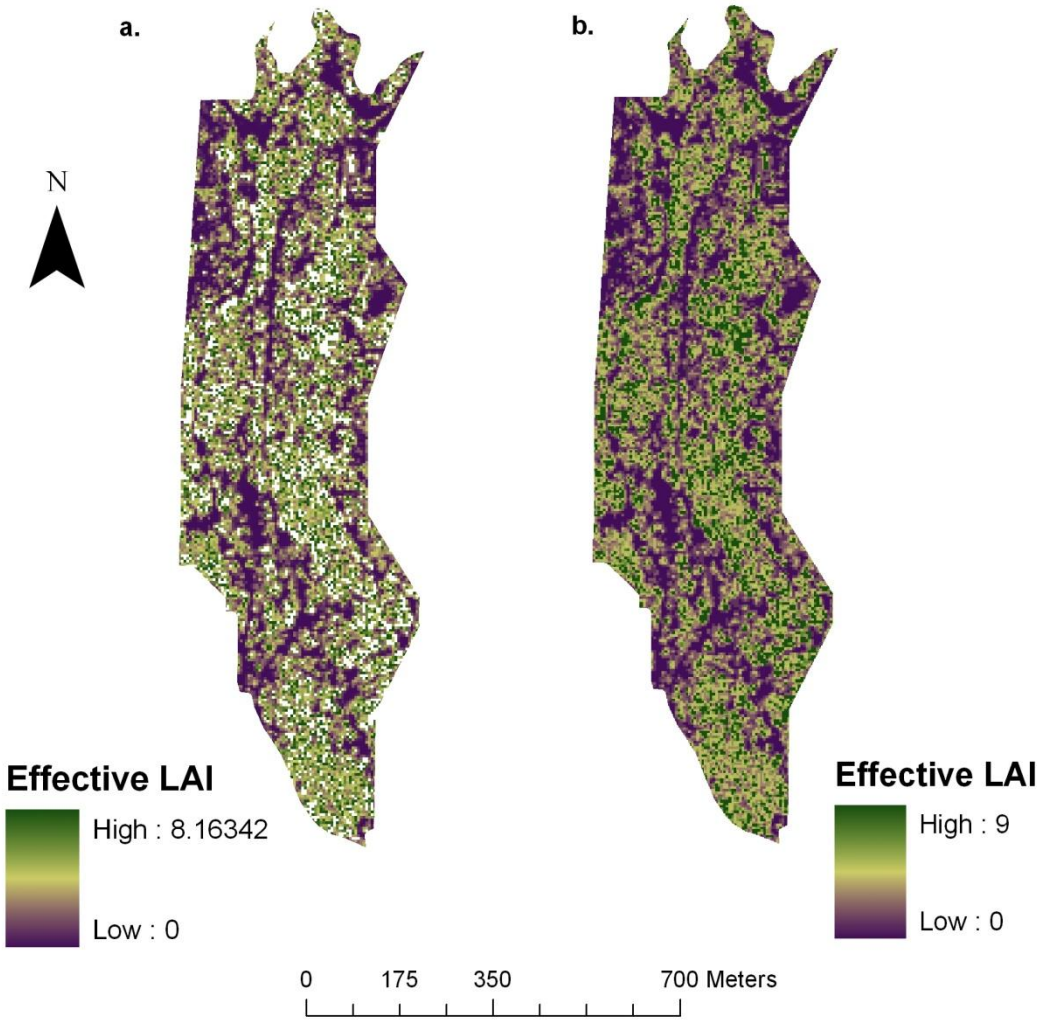

Figure 7: Estimates of LAI_E within the area of study with (a.) pixels with no ground returns shown as white and (b.) pixels with no ground returns set to an LAI_E of 9 and interpolated using the IDW technique.

Figure 8.a. is a grid created by running the IDW interpolation on the grid from Fig 7.a. with no data pixels included. This produced a continuous grid that can serve as an input for ecological models, but likely underestimates LAI_E because pixels could not be assigned values larger than 8.16.

Figure 8.b. was created by iteratively increasing the pixel size of the raster grid of ground returns until a continuous grid was created where every pixel had a value

greater or equal to one. This was point was reached with a pixel size of 16 m. This provided a dataset that model E could be run to produce a continuous estimate of LAI_E. The obvious drawback is the reduction in resolution, and this may or may not be a serious problem depending on the application.

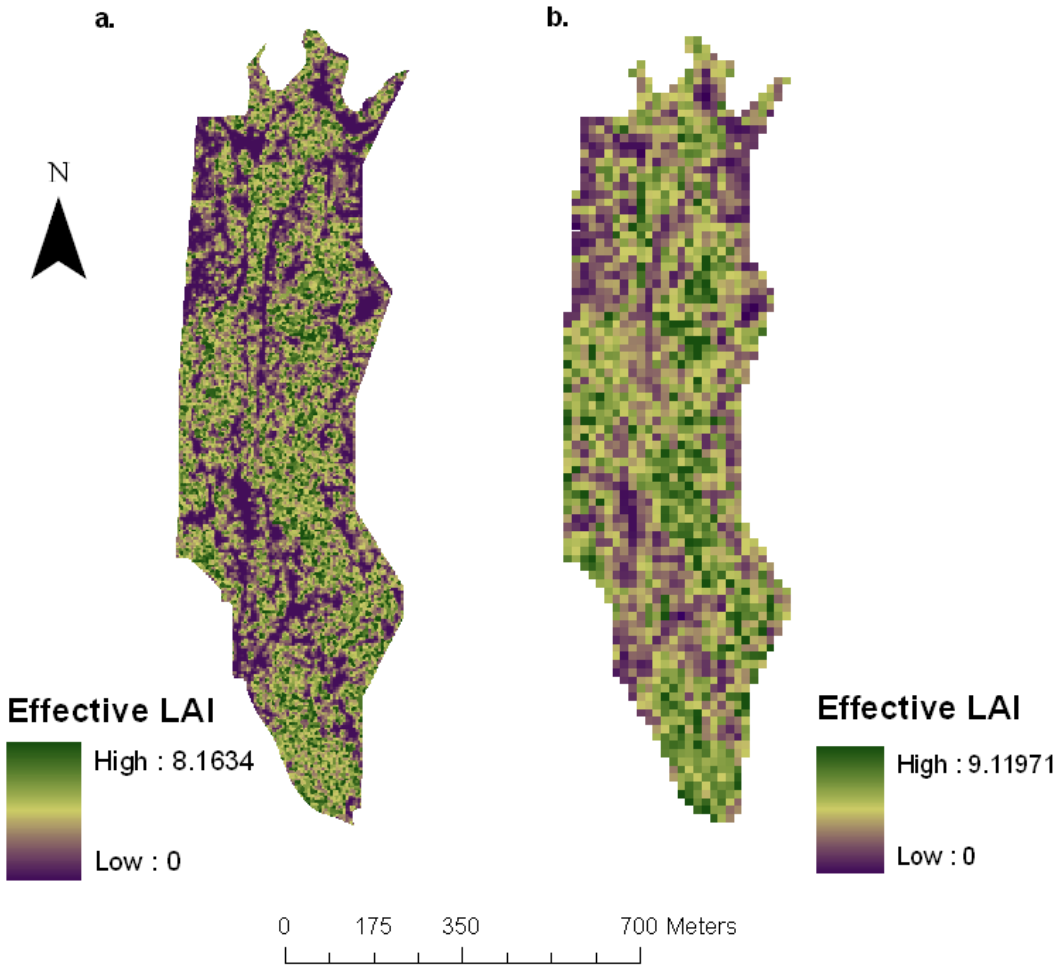

Figure 8: Estimates of LAI_E within the area of study with (a.) pixels interpolated on the raw modeled output using the IDW technique and (b) 16 m pixels.

The maps from Fig. 7 and 8 can now be used as an input into various models requiring estimates of LAI. Each has its drawbacks, but Figure 8.b. is the map most likely to contain the least amount of error because it does not require assumptions or

produce obvious underestimates. It is important to note, though, that the range of pixel values in all four maps is larger than the range obtained from hemispherical photographs used in parameterizing the model. With the increase in residual scatter seen at these high LAI_E values in Fig. 5.E., the error associated with the larger values in Figures 7 and 8 may also be large. Nothing definitive can be quantified without further validation. Care must also be taken to account for the fact that these are estimates of LAI_E and not true LAI.

Future research or analysis can be undertaken to use these maps as a source of data for models of carbon sequestration, rainfall interception, pollution interception, or other ecological functions. If future LiDAR flights are acquired over the WPA, these maps can also be used to assess changes in LAI_E over time, and thus changes in the ecological functions provided by the WPA.

End Notes

Asner, G.P., Scurlock, J.M.O. and A. Hicke, J., 2003. Global synthesis of leaf area index observations: implications for ecological and remote sensing studies, pp. 191-205.

Chen, J.M., Rich, P.M., Gower, S.T., Norman, J.M. and Plummer, S., 1997. Leaf area index of boreal forests: Theory, techniques, and measurements. Journal of Geophysical Research-Atmospheres, 102(D24): 29429-29443.

Gower, S.T., Kucharik, C.J. and Norman, J.M., 1999. Direct and Indirect Estimation of Leaf Area Index, fAPAR, and Net Primary Production of Terrestrial Ecosystems. Remote Sensing of Environment, 70(1): 29-51.

Hanssen, K.H. and Solberg, S., 2007. Assessment of defoliation during a pine sawfly outbreak: Calibration of airborne laser scanning data with hemispherical photography. Forest Ecology and Management, 250(1-2): 9-16.

Leblanc, S.G., 2006. Digital hemispherical photography manual. Natural Resources Canada, Canada Centre for Remote Sensing.

Leblanc, S.G., Chen, J.M., Fernandes, R., Deering, D.W. and Conley, A., 2005. Methodology comparison for canopy structure parameters extraction from digital hemispherical photography in boreal forests. Agricultural and Forest Meteorology, 129(3-4): 187-207.

Lefsky, M.A. et al., 1999. Lidar remote sensing of the canopy structure and biophysical properties of Douglas-fir western hemlock forests. Remote Sensing of Environment, 70(3): 339-361.

Lefsky, M.A., Cohen, W.B., Parker, G.G. and Harding, D.J., 2002. Lidar remote sensing for ecosystem studies. Bioscience, 52(1): 19-30.

Lim, K., Treitz, P., Baldwin, K., Morrison, I. and Green, J., 2003. Lidar remote sensing of biophysical properties of tolerant northern hardwood forests. Canadian Journal of Remote Sensing, 29(5): 658-678.

Lüdeke, M., Janecek, A. and Kohlmaier, G.H., 1991. Modelling the seasonal CO_2 uptake by land vegetation using the global vegetation index. Tellus, 43B: 188-196.

McGaughey, R.J., 2007. FUSION/LDV: software for LIDAR data analysis and visualization. United States Department of Agriculture, Forest Service, Pacific Northwest Research Station.

Melillo, J.M. et al., 1993. Global climate-change and terrestrial net primary production. Nature, 363(6426): 234-240.

Monsi, M. and Saeki, T., 1952. U¨ber den Lichtfaktor in den Pflanzengesellschaften und seine Bedeutung fu¨r die Stoffproduktion.Japanese Journal of Botany, 14: 22-52.

Morsdorf, F., Kotz, B., Meier, E., Itten, K.I. and Allgower, B., 2006. Estimation of LAI and fractional cover from small footprint airborne laser scanning data based on gap fraction. Remote Sensing of Environment, 104(1): 50-61.

Nowak, D.J., 1996. Estimating leaf area and leaf biomass of open-grown deciduous urban trees. Forest Science, 42(4): 504-507.

Nowak, D.J. and Crane, D.E., 1998. The urban forest effects (UFORE) model: quantifying urban forest structure and functions. In: M. Hansen and T. Burk (Editors), IUFRO. Integrated tools for natural resources inventories in the 21st century. U.S. Department of Agriculture, Forest Service, North Central Forest Experiment Station, Boise, ID, pp. 714-720.

Pierce, L.L. and Running, S.W., 1988. Rapid Estimation of Coniferous Forest Leaf Area Index Using a Portable Integrating Radiometer. Ecology, 69(6): 1762-1767.

Riaño, D., Valladares, F., Condes, S. and Chuvieco, E., 2004. Estimation of leaf area index and covered ground from airborne laser scanner (Lidar) in two contrasting forests. Agricultural and Forest Meteorology, 124(3-4): 269-275.

Solberg, S., Naesset, E., Hanssen, K.H. and Christiansen, E., 2006. Mapping defoliation during a severe insect attack on Scots pine using airborne laser scanning. Remote Sensing of Environment, 102(3-4): 364-376.

Thomas, S.C. and Winner, W.E., 2000. Leaf area index of an old-growth Douglas-fir forest estimated from direct structural measurements in the canopy. Canadian Journal of Forest Research-Revue Canadienne De Recherche Forestiere, 30(12): 1922-1930.

Vose, J.M., Sullivan, N.H., Clinton, B.D. and Bolstad, P.V., 1995. Vertical Leaf-Area Distribution, Light Transmittance, and Application of the Beer-Lambert Law in 4

Mature Hardwood Stands in the Southern Appalachians. Canadian Journal of Forest Research-Revue Canadienne De Recherche Forestiere, 25(6): 1036-1043.

Wang, Q., Adiku, S., Tenhunen, J. and Granier, A., 2005. On the relationship of NDVI with leaf area index in a deciduous forest site. Remote Sensing of Environment, 94(2): 244-255.

Zhang, Y.Q., Chen, J.M. and Miller, J.R., 2005. Determining digital hemispherical photograph exposure for leaf area index estimation. Agricultural and Forest Meteorology, 133(1-4): 166-181.

Bibliography

Andersen, H., McGaughey, R.J. and Reutebuch, S.E., 2005. Estimating forest canopy fuel parameters using LIDAR data. Remote Sensing of Environment, 94(4): 441-449.

Asner, G.P., Scurlock, J.M.O. and A. Hicke, J., 2003. Global synthesis of leaf area index observations: implications for ecological and remote sensing studies, pp. 191-205.

Brack, C.L., 2002. Pollution mitigation and carbon sequestration by an urban forest. Environmental Pollution, 116: S195-S200.

Bréda, N.J.J., 2003. Ground-based measurements of leaf area index: a review of methods, instruments and current controversies. Journal of Experimental Botany, 54(392): 2403-2417.

Case, M.J. and Peterson, D.L., 2005. Fine-scale variability in growth-climate relationships of Douglas-fir, North Cascade Range, Washington. Canadian Journal of Forest Research-Revue Canadienne De Recherche Forestiere, 35(11): 2743-2755.

Chen, J.M. and Black, T.A., 1991. Measuring leaf-area index of plant canopies with branch architecture. Acricultural and Forest Meterology, 57: 1-12.

Chen, J.M. and Black, T.A., 1992. Defining Leaf-Area Index for Non-Flat Leaves. Plant Cell and Environment, 15(4): 421-429.

Chen, J.M., Black, T.A. and Adams, R.S., 1991. Evaluation of Hemispherical Photography for Determining Plant-Area Index and Geometry of a Forest Stand. Agricultural and Forest Meteorology, 56(1-2): 129-143.

Chen, J.M. and Cihlar, J., 1996. Retrieving leaf area index of boreal conifer forests using landsat TM images. Remote Sensing of Environment, 55(2): 153-162.

Chen, J.M., Rich, P.M., Gower, S.T., Norman, J.M. and Plummer, S., 1997. Leaf area index of boreal forests: Theory, techniques, and measurements. Journal of Geophysical Research-Atmospheres, 102(D24): 29429-29443.

Chen, X.X., Vierling, L., Rowell, E. and DeFelice, T., 2004. Using lidar and effective LAI data to evaluate IKONOS and Landsat 7 ETM+ vegetation cover estimates in a ponderosa pine forest. Remote Sensing of Environment, 91(1): 14-26.

Chen, Y.H., Shi, P.J., Li, X.B., Chen, J. and Li, J., 2006. A combined approach for estimating vegetation cover in urban/suburban environments from remotely sensed data. Computers & Geosciences, 32(9): 1299-1309.

Dwyer, J.F., McPherson, E.G., Schroeder, H.W. and Rowntree, R.A., 1992. Assessing the benefits and costs of the urban forest. Journal of Arboriculture, 18(5): 227-234.

Evans, G.C. and Coombe, D.E., 1959. Hemispherical and woodland canopy photography and the light climate. Journal of Ecology, 47(1): 103-113.

Farid, A., Goodrich, D.C., Bryant, R. and Sorooshian, S., 2007. Using airborne lidar to predict leaf area index in cottonwood trees and refine riparian water-use estimates. Journal of Arid Environments.

Fassnacht, K.S., Gower, S.T., MacKenzie, M.D., Nordheim, E.V. and Lillesand, T.M., 1997. Estimating the leaf area index of North Central Wisconsin forests using the Landsat Thematic Mapper. Remote Sensing of Environment, 61(2): 229-245.

Fensholt, R., Sandholt, I. and Rasmussen, M.S., 2004. Evaluation of MODIS LAI, fAPAR and the relation between fAPAR and NDVI in a semi-arid environment using in situ measurements. Remote Sensing of Environment, 91(3-4): 490-507.

Frazer, G., Trofymow, J. and Lerzman, K., 1997. A method for estimating canopy openness, effective leaf area index and photosynthetically active photon flux density using hemispherical photography and computerized image analysis techniques. Natural Resources Canada, Canadian Forest Service, Pacific Forestry Centre, Victoria, BC.

Goodwin, N.R., Coops, N.C. and Culvenor, D.S., 2007. Development of a simulation model to predict LiDAR interception in forested environments. Remote Sensing of Environment, 111(4): 481-492.

Gower, S.T., Kucharik, C.J. and Norman, J.M., 1999. Direct and Indirect Estimation of Leaf Area Index, fAPAR, and Net Primary Production of Terrestrial Ecosystems. Remote Sensing of Environment, 70(1): 29-51.

Hanssen, K.H. and Solberg, S., 2007. Assessment of defoliation during a pine sawfly outbreak: Calibration of airborne laser scanning data with hemispherical photography. Forest Ecology and Management, 250(1-2): 9-16.

Henning, J.G. and Radtke, P.J., 2006. Detailed stem measurements of standing trees from ground-based scanning lidar. Forest Science, 52(1): 67-80.

Henning, J.G. and Radtke, P.J., 2006. Ground-based laser imaging for assessing three-dimensional forest canopy structure. Photogrammetric Engineering and Remote Sensing, 72(12): 1349-1358.

Hopkinson, C., Chasmer, L., Young-Pow, C. and Treitz, P., 2004. Assessing forest metrics with a ground-based scanning lidar. Canadian Journal of Forest Research-Revue Canadienne De Recherche Forestiere, 34(3): 573-583.

Hosoi, F. and Omasa, K., 2006. Voxel-based 3-D modeling of individual trees for estimating leaf area density using high-resolution portable scanning lidar. Ieee Transactions on Geoscience and Remote Sensing, 44(12): 3610-3618.

Jensen, R.R. and Hardin, P.J., 2005. Estimating urban leaf area using field measurmenets and satellite remote sensing data. Journal of Arboriculture, 31(1): 21-27.

Kim, S.H. et al., 2006. Canopy photosynthesis, evapotranspiration, leaf nitrogen, and transcription profiles of maize in response to CO2 enrichment. Global Change Biology, 12(3): 588-600.

Kimball, J.S., Thornton, P.E., White, M.A. and Running, S.W., 1997. Simulating forest productivity and surface-atmospher carbon exchange in the BOREAS study region. Tree Physiology, 17(8-9): 589-599.

Landsberg, J.J. and Waring, R.H., 1997. A generalised model of forest productivity using simplified concepts of radiation-use efficiency, carbon balance and partitioning. Forest Ecology and Management, 95(3): 209-228.

Leblanc, S.G., 2006. Digital hemispherical photography manual. Natural Resources Canada, Canada Centre for Remote Sensing.

Leblanc, S.G., Chen, J.M., Fernandes, R., Deering, D.W. and Conley, A., 2005. Methodology comparison for canopy structure parameters extraction from digital hemispherical photography in boreal forests. Agricultural and Forest Meteorology, 129(3-4): 187-207.

Lefsky, M.A. et al., 1999. Lidar remote sensing of the canopy structure and biophysical properties of Douglas-fir western hemlock forests. Remote Sensing of Environment, 70(3): 339-361.

Lefsky, M.A., Cohen, W.B., Parker, G.G. and Harding, D.J., 2002. Lidar remote sensing for ecosystem studies. Bioscience, 52(1): 19-30.

Lefsky, M.A., Harding, D., Cohen, W.B., Parker, G. and Shugart, H.H., 1999. Surface lidar remote sensing of basal area and biomass in deciduous forests of eastern Maryland, USA. Remote Sensing of Environment, 67(1): 83-98.

Lim, K., Treitz, P., Baldwin, K., Morrison, I. and Green, J., 2003. Lidar remote sensing of biophysical properties of tolerant northern hardwood forests. Canadian Journal of Remote Sensing, 29(5): 658-678.

Lovell, J.L., Jupp, D.L.B., Culvenor, D.S. and Coops, N.C., 2003. Using airborne and ground-based raning lidar to measure canopy structure in Australian forests. Canadian Journal of Remote Sensing, 29(5): 607-622.

Lüdeke, M., Janecek, A. and Kohlmaier, G.H., 1991. Modelling the seasonal CO_2 uptake by land vegetation using the global vegetation index. Tellus, 43B: 188-196.

McGaughey, R.J., 2007. FUSION/LDV: software for LIDAR data analysis and visualization. United States Department of Agriculture, Forest Service, Pacific Northwest Research Station.

McPherson, E.G., 1998. Atmospheric carbon dioxide reduction by Sacramento's urban forest. Journal of Arboriculture, 24(4): 215-223.

Melillo, J.M. et al., 1993. Global climate-change and terrestrial net primary production. Nature, 363(6426): 234-240.

Miller, J.B., 1967. A formula for average foliage density. Australian Journal of Botany, 15(1): 141-144.

Monsi, M. and Saeki, T., 1952. U¨ber den Lichtfaktor in den Pflanzengesellschaften und seine Bedeutung fu¨r die Stoffproduktion.Japanese Journal of Botany, 14: 22-52.

Morsdorf, F., Kotz, B., Meier, E., Itten, K.I. and Allgower, B., 2006. Estimation of LAI and fractional cover from small footprint airborne laser scanning data based on gap fraction. Remote Sensing of Environment, 104(1): 50-61.

Myeong, S., Nowak, D.J. and Duggin, M.J., 2006. A temporal analysis of urban forest carbon storage using remote sensing. Remote Sensing of Environment, 101(2): 277-282.

Norby, R.J., Wullschleger, S.D., Gunderson, C.A., Johnson, D.W. and Ceulemans, R., 1999. Tree responses to rising CO2 in field experiments: implications for the future forest. Plant Cell and Environment, 22(6): 683-714.

Nowak, D.J., 1993. Atmospheric carbon reduction by urban trees. Journal of Enivronmental Management, 37: 207-217.

Nowak, D.J., 1996. Estimating leaf area and leaf biomass of open-grown deciduous urban trees. Forest Science, 42(4): 504-507.

Nowak, D.J., C., S.J., Sisinni, S.M. and Luley, C.J., 2002. Effects of urban tree management and species selection on atmospheric carbon dioxide. Journal of Arboriculture, 28(3): 113-122.

Nowak, D.J. and Crane, D.E., 1998. The urban forest effects (UFORE) model: quantifying urban forest structure and functions. In: M. Hansen and T. Burk (Editors), IUFRO. Integrated tools for natural resources inventories in the 21st century. U.S. Department of Agriculture, Forest Service, North Central Forest Experiment Station, Boise, ID, pp. 714-720.

Nowak, D.J. et al., 1996. Measuring and analyzing urban tree cover. Landscape and Urban Planning, 36(1): 49-57.

Parker, G.G., Harding, D.J. and Berger, M.L., 2004. A portable LIDAR system for rapid determination of forest canopy structure. Journal of Applied Ecology, 41(4): 755-767.

Peper, P.J. and McPherson, E.G., 1998. Comparison of five methods for estimating leaf area index of open-grown deciduous trees. Journal of Arboriculture, 24(2): 96-111.

Peper, P.J. and McPherson, E.G., 2003. Evaluation of four methods for estimating leaf area of isolated trees. Urban Forestry & Urban Greening, 2(1): 19-29.

Pierce, L.L. and Running, S.W., 1988. Rapid Estimation of Coniferous Forest Leaf Area Index Using a Portable Integrating Radiometer. Ecology, 69(6): 1762-1767.

Popescu, S.C., Wynne, R.H. and Scrivani, J.A., 2004. Fusion of small-footprint lidar and multispectral data to estimate plot-level volume and biomass in deciduous and pine forests in Virginia, USA. Forest Science, 50(4): 551-565.

Pouyat, R., Groffman, P., Yesilonis, I. and Hernandez, L., 2002. Soil carbon pools and fluxes in urban ecosystems. Environmental Pollution, 116: S107-S118.

Riano, D. et al., 2006. A simple model to calculate leaf area index from lidar data, American Geophysical Union, Fall Meeting.

Riaño, D., Valladares, F., Condes, S. and Chuvieco, E., 2004. Estimation of leaf area index and covered ground from airborne laser scanner (Lidar) in two contrasting forests. Agricultural and Forest Meteorology, 124(3-4): 269-275.

Roberts, D.A. et al., 2004. Spectral and structural measures of northwest forest vegetation at leaf to landscape scales. Ecosystems, 7: 545-562.

Roberts, S.D. et al., 2005. Estimating individual tree leaf area in loblolly pine plantations using LiDAR-derived measurements of height and crown dimensions. Forest Ecology and Management, 213(1-3): 54-70.

Roth, E.B., Slatton, K.C. and Cohen, M.J., 2007. On the potential for high-resolution lidar to improve rainfall interception estimates in forest ecosystems. Frontiers in Ecology and the Environment, 5(8): 421-428.

Solberg, S., Naesset, E., Hanssen, K.H. and Christiansen, E., 2006. Mapping defoliation during a severe insect attack on Scots pine using airborne laser scanning. Remote Sensing of Environment, 102(3-4): 364-376.

Thies, M., Pfeifer, N., Winterhalder, D. and Gorte, B.G.H., 2004. Three-dimensional reconstruction of stems for assessment of taper, sweep and lean based on laser scanning of standing trees. Scandinavian Journal of Forest Research, 19(6): 571-581.

Thomas, S.C. and Winner, W.E., 2000. Leaf area index of an old-growth Douglas-fir forest estimated from direct structural measurements in the canopy. Canadian Journal of Forest Research-Revue Canadienne De Recherche Forestiere, 30(12): 1922-1930.

Van der Zande, D., Hoet, W., Jonckheere, L., van Aardt, J. and Coppin, P., 2006. Influence of measurement set-up of ground-based LiDAR for derivation of tree structure. Agricultural and Forest Meteorology, 141(2-4): 147-160.

Vose, J.M., Sullivan, N.H., Clinton, B.D. and Bolstad, P.V., 1995. Vertical Leaf-Area Distribution, Light Transmittance, and Application of the Beer-Lambert Law in 4 Mature Hardwood Stands in the Southern Appalachians. Canadian Journal of Forest Research-Revue Canadienne De Recherche Forestiere, 25(6): 1036-1043.

Wang, Q., Adiku, S., Tenhunen, J. and Granier, A., 2005. On the relationship of NDVI with leaf area index in a deciduous forest site. Remote Sensing of Environment, 94(2): 244-255.

Watt, P.J. and Donoghue, D.N.M., 2005. Measuring forest structure with terrestrial laser scanning. International Journal of Remote Sensing, 26(7): 1437-1446.

Zhang, Y.Q., Chen, J.M. and Miller, J.R., 2005. Determining digital hemispherical photograph exposure for leaf area index estimation. Agricultural and Forest Meteorology, 133(1-4): 166-181.

Appendix A: List of Acronyms

CC: Canopy Classes

CGV: Closed Gap Volume

CV: Canopy Volume

DEM: Digital Elevation Model

DGPS: Differential-corrected Global Positioning System

DHP: Digital Hemispherical Photography

F_C: Fractional Cover

FCV: Filled Canopy Volume

GPP: Gross Primary Productivity

GPS: Global Positioning System

H: Mean Canopy Height

IDW: Inverse Distance Weighted

LAI: Leaf Area Index

LAI_E: Effective Leaf Area Index

LiDAR: Light Detection and Ranging

Model A: $LAI_E = \alpha + \beta$ MRE

Model B: $LAI_E = \alpha + \beta CV$

Model C: $LAI_E = \alpha + \beta$ –PCH

Model D: $LAI_E = \alpha + \beta F_c (\sum R_{C1}/(\sum R_{C2} + \sum R_{C3}))$

Model E: $LAI_E = \beta - \ln(R_G/R_G + R_C)$

MRE: Mean Return Elevation

PCH: Percent Canopy Hits

R_C: Canopy Returns

R_{C1}: Canopy First Returns

R_{C2}: Canopy Second Returns

$R_{C3:}$ Canopy Third Returns

R_{CL}: Canopy Last Returns

R_{CO}: Canopy Only Returns

R_G: Ground Returns

R_{IR}: Reflectance in the Infrared Wavelength

R_{NIR}: Reflectance in the Near Infrared Wavelength

SE: Standard Error

TIN: Triangular Irregular Network

WPA: Washington Park Arboretum

Appendix B: Users Guide to Hemispherical Photograph Acquisition and Analysis

The purpose of this supplement is to record the method used in this study for acquiring and analyzing hemispherical photographs. There are many sources of error in this process, and this presents the detailed method used to produce estimates of LAI_E.

Acquisition

1. The camera used was Nikon CoolPix 4500 with a Nikon FC-E8 Fisheye lens. This camera was also used in the development of the method for acquiring hemispherical photographs in Zhang et al. (2005). If other cameras are to be used, this guide should be modified.
2. The camera was put into Fisheye mode and manual focus mode.
3. The aperture was set to 5.3
4. The camera was placed on a 1 m tall tripod, brought into an open field and leveled. The shutter speed was then adjusted until the light meter was two "clicks" to the right of the suggested level.
5. The camera was then brought to the plot location, leveled, set to face magnetic north, and set to timer mode.
6. The shutter was depressed and the operator ducked to be out of the field of view of the photograph.
7. If light levels are changing rapidly (as they do at dawn and dusk), the camera should be brought into an open field at regular interviews to adjust the shutter speed using the methodology in step 4.

Analysis

1. Digital Hemispherical Photography (DHP) software was used for the analysis. This software can be obtained for free from Sylvain G. LeBlanc (Sylvain.Leblanc@CCRS.NRCan.gc.ca).

2. Click “Browse Input” and select the image file of the photograph.
3. You will be prompted to select the camera used in obtaining the photograph. If not prompted, select the camera in the drop down menu. If the camera is not shown, consult the software’s user manual.
4. Click “Blue” in Input Options.
5. For the CoolPix 4500, enter 2.2 for Gamma. Consult the software manual if using a different camera.
6. The software breaks the photograph into 10 annulus rings. You can switch between rings using “Up” and “Down”.
7. Make sure “Histogram Logarithm View” is checked
8. Select “Down” until ring 10 is selected.
9. A histogram of the pixel values in the blue band is shown at the right, on a logarithmic scale. The sliders above and below the histogram can be moved to se the thresholds for “foliage” pixels, “mixed” pixels, and “sky” pixels.
10. Each ring will follow a similar pattern in its histogram. There will be a steep peak at the left leveling off to a near linear area, followed by a steep peak at the right.
11. The bottom slider should be set at the left edge of the linear area, at the point where the “slope” of the histogram moves from linear to exponential.
12. The top slider should be set at the right edge of the linear area, at the point where the “slope” of the histogram moves from linear to exponential.
13. If the histogram is not clear, the thresholds can be adjusted using visual inspection of the ring. The area at the left displays the image of the ring. Higher resolution can be achieved using “Full Resolution” and areas denoted as “mixed pixels” will be displayed in green if “Gaps Colour Code” is selected. By moving the sliders, inspecting the histogram, and inspecting the image, the proper threshold can be set.
14. Continue on to each of the next nine rings, following steps 11-13.

15. When finished, LAI_E estimates can be retrieved by entering the number of rings the analysis should process in the box “Rings #.” Select “Process” to retrieve the estimates.
16. The upper right window will display the LAI_E (displayed as PAI_e) at the top column for the rings selected. It will also display the individual LAI_E for each of the 10 rings below that.
17. The thresholds for each photo will be saved in a text file and can be accessed at a later date.
18. The output can also be exported to TRACwin. See the user manual for more information.